

X-ray diffraction from shock-loaded polycrystals

Damian C. Swift*

*P-24 Plasma Physics, Los Alamos National Laboratory,
MS E526, Los Alamos, New Mexico 87545, USA*

(Dated: February 19, 2006; revised July 4, 2007)

X-ray diffraction was demonstrated from shock-compressed polycrystalline metal on nanosecond time scales. Laser ablation was used to induce shock waves in polycrystalline foils of Be, 25 to 125 μm thick. A second laser pulse was used to generate a plasma x-ray source by irradiation of a Ti foil. The x-ray source was collimated to produce a beam of controllable diameter, and the beam was directed at the Be sample. X-rays were diffracted from the sample, and detected using films and x-ray streak cameras. The diffraction angle was observed to change with shock pressure. The diffraction angles were consistent with the uniaxial (elastic) and isotropic (plastic) compressions expected for the loading conditions used. Polycrystalline diffraction will be used to measure the response of the crystal lattice to high shock pressures and through phase changes.

PACS numbers: 07.35.+k, 62.50.+p, 61.10.Nz, 07.85.Jy

Keywords: shock, laser ablation, x-ray diffraction, plasticity, phase transitions

I. INTRODUCTION

Shock wave experiments and static presses such as diamond anvil cells are the principal techniques for investigating the behavior of materials at high pressures [1]. Shock wave experiments are particularly important when investigating, and developing models of, the response of materials to dynamic loading such as the shocks themselves. One of the key measurements in static presses is diffraction, which provides direct observation of the compression and strain of the crystal lattice, and can be used to detect and identify phase transitions. These measurements are important comparisons with theoretical predictions such as electronic structure calculations.

Diffraction in static presses is routinely performed from samples which are single crystals or polycrystalline ensembles [1]. In shock wave experiments, the usual experimental measurements include the speed of the shock wave and the material speed behind the shock. Such observations can be used to infer the mechanical equation of state and some aspects of plastic flow. Diffraction data from shocked samples are potentially extremely valuable as direct measurements of the elastic compression of the crystal lattice, the onset of plastic flow, phase transitions, and the density of crystal defects such as dislocations. The width of the diffraction lines may allow the temperature of the shocked material to be deduced, which is a long-standing problem in shock physics.

X-ray diffraction has been performed in shock wave experiments, using single crystal samples loaded by projectile impact [2, 3] and by laser ablation [4]. The length of time for which the high pressure state persists is short, typically for microseconds in projectile impact experiments and nanoseconds or less for ablative loading. It is difficult to generate x-rays with sufficient power to ac-

quire a diffraction pattern on these time scales, and to synchronize the x-rays with the shock. X-ray diffraction patterns have been obtained by integrating the signal as samples are shocked repetitively [5, 6], but these experiments were performed using single crystals loaded by ablation from sub-picosecond laser pulses. It is not practical to perform large number of repeat measurements with current projectile guns and high energy lasers, and it is in any case highly desirable to collect the diffraction pattern during a single, well-characterized shock event.

Diffraction from shocked polycrystalline material has not been reported previously, but is desirable in several respects. Using a single crystal, the point at which diffraction occurs moves across the sample as the lattice spacing changes. For high compressions, it can be difficult to ensure that both the unshocked and shocked lines can be accommodated over the finite width of the shocked region (Fig. 1). In contrast, polycrystalline diffraction is best arranged from a single point (or small area) of the sample, which does not move with compression. Another compelling reason is that, even if a sample is initially a single crystal, if it undergoes a phase transition then the daughter phase may be polycrystalline. For many materials, polycrystalline samples are far easier to obtain than are single crystals, and it is desirable to study the properties of materials in the form in which they are used in engineering applications. It is also interesting to study the effect of grain size and sample texture on properties such as the dynamics of phase changes.

We have performed x-ray diffraction experiments on shock-loaded single crystals of a variety of materials, notably Si [4, 7] and Be [8]. Be-based alloys are of technological interest as the deuterium-tritium fuel capsule for inertial confinement fusion (ICF) [9, 10, 11]. Our experiments on Be investigate the anisotropy of plastic response under dynamic loading, and phase transitions including melting. As well as their technological significance, time-resolved x-ray diffraction data from these experiments are valuable in understanding plasticity in

*Electronic address: dswift@lanl.gov

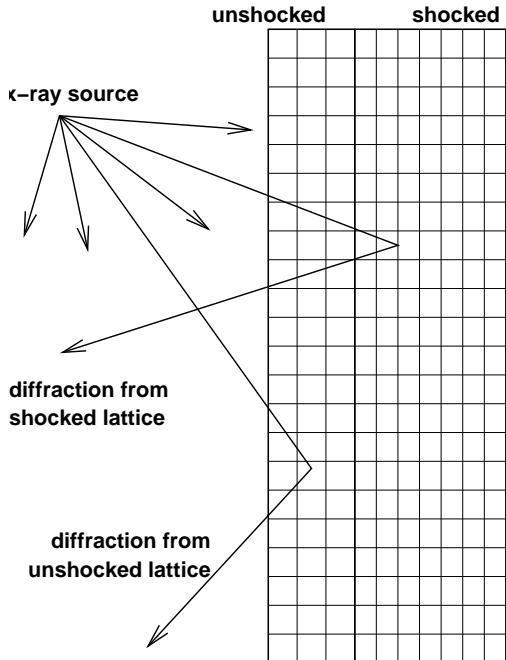


FIG. 1: Schematic of transient x-ray diffraction from a single crystal sample, illustrating diffraction from different points at different compressions.

hexagonal metals and the dynamics of melting. Shock loading was induced by laser ablation (Fig. 2): the loading history is often less simple and less well-characterized than is the case for projectile impact experiments, but laser-induced shocks are far easier to synchronize with laser-powered x-ray sources. They are also more appropriate for the length and time scales of interest for ICF: $\sim 100 \mu\text{m}$ and 1 ns. We have developed an accurate predictive capability to relate the pressure history of the shock to the irradiance history of the laser pulse [12, 13]. Radiation hydrodynamics simulations can be used to understand the loading history, and to adjust the temporal structure of the pulse to induce a constant drive pressure and hence a better-characterized shock.

II. LASER ABLATION EXPERIMENTS

These experiments were performed at the TRIDENT laser facility at Los Alamos National Laboratory. TRIDENT is based around a Nd:glass laser with a fundamental wavelength of 1054 nm. To improve the coupling to matter and reduce the risk of damage to the laser from backscatter of the fundamental, for these experiments the beams were frequency-doubled to 527 nm. Each sample was loaded by irradiation using the one beam of the laser; pressure was generated by ablation of material from the irradiated surface (Fig. 2).

Because of the experimental configuration used (specifically, the design of the nose of the x-ray streak cam-

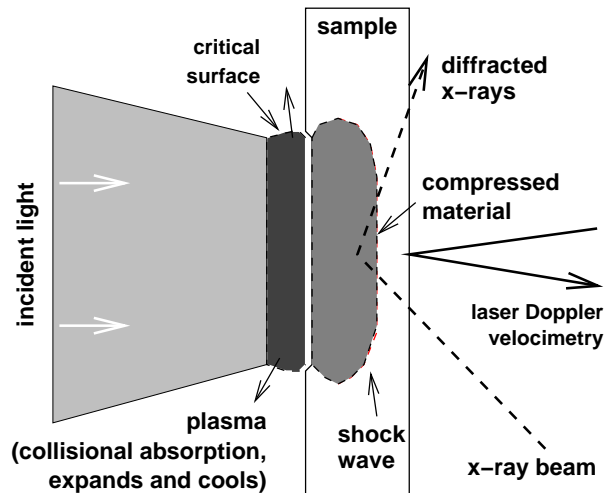


FIG. 2: Schematic of shock generation by laser ablation.

eras), it was difficult to acquire velocimetry and x-ray diffraction data at the same time. Two types of experiment were performed: a series with no diffraction measurements in which the velocity history of the opposite surface (across the thin direction) was measured using line-imaging Doppler velocimetry for a wide range of irradiance histories [14, 15], and a series of diffraction measurements in which the velocity history was measured on only some shots. The irradiance history was measured in all cases, so the loading history could be calculated using radiation hydrodynamics and continuum mechanics simulations.

X-rays were generated by irradiating a thin metal foil with a second laser pulse, tightly-focused, to produce a hot plasma. The resulting x-rays were collimated to illuminate the center of the sample with a narrow beam. In our previous experiments with single crystals [4, 7, 8], diffraction produced cones of x-rays with a virtual apex at the x-ray source, reflected by the diffracting plane in the sample. For a collimated x-ray beam and a polycrystalline sample, diffraction produces a series of cones whose axis is the incident x-ray beam and apex is the diffracting point on the sample [16]. Films and x-ray streak cameras were positioned to record photons diffracted around 90° from the incident beam, where powder diffraction from Be would produce a signal. The slit of the streak camera was parallel to the x-ray beam, so a given change in powder diffraction angle would produce the greatest change in line position. For polycrystal diffraction from thin samples, the angle of the sample with respect to the x-rays is not important. In these experiments, the sample was mounted normal to the drive beam, which was at 136° from the x-ray beam. (Fig. 3.)

The laser beam used to induce the shock driving beam and the laser beam used to generate x-rays were both driven from the same master oscillator, so they shared the same duration and un-amplified pulse shape, though the

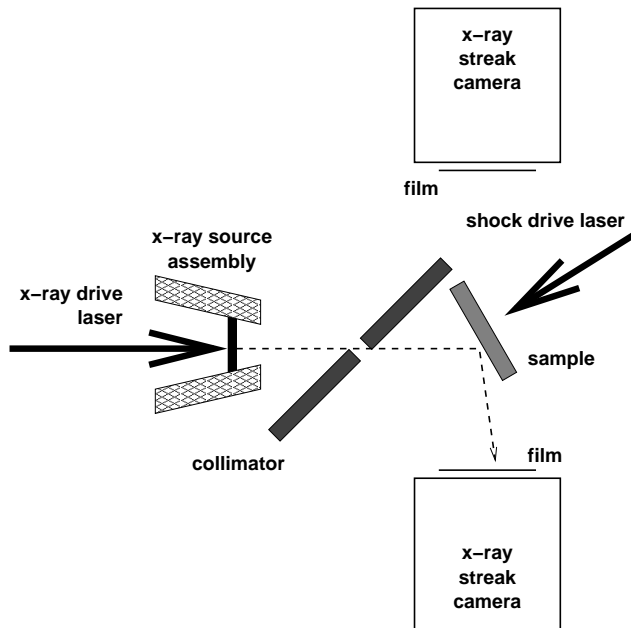


FIG. 3: Schematic of experimental layout (not to scale). The slit in each x-ray streak camera was in the plane of the diagram.

energies were controlled independently. The pulse shape was chosen to optimize the shock drive (keeping the pressure as constant as possible in time); the energy of the x-ray generating pulse was chosen to optimize the spectrum and intensity of x-rays. The timing of the x-rays was defined with respect to the shock drive, by changing the path length of the x-ray driving beam. Typical delays were ~ 2 ns.

A. Sample material

Be foils were obtained from Goodfellow Inc, of 99.8% purity (the maximum supplied). These were rolled foils, with significant texture. The texture was investigated by obtaining x-ray orientation maps of a couple of sample foils. The scattering efficiency of Be is low, so the thicker foils ($125\ \mu\text{m}$) were used in these measurements. The foils were found to be oriented preferentially so that normals to the (0001) planes were distributed around the normal to the foil, equivalent to a rocking curve a couple of tens of degrees wide. The (10 $\bar{1}$ 0) planes were distributed with normals in the plane of the sample, though with significant variation in this azimuthal distribution, reflecting the directions in which the foil was rolled. (Fig. 4.)

B. Target assembly

A re-usable holder was used to locate the sample and x-ray source reproducibly for each shot (Fig. 5). The

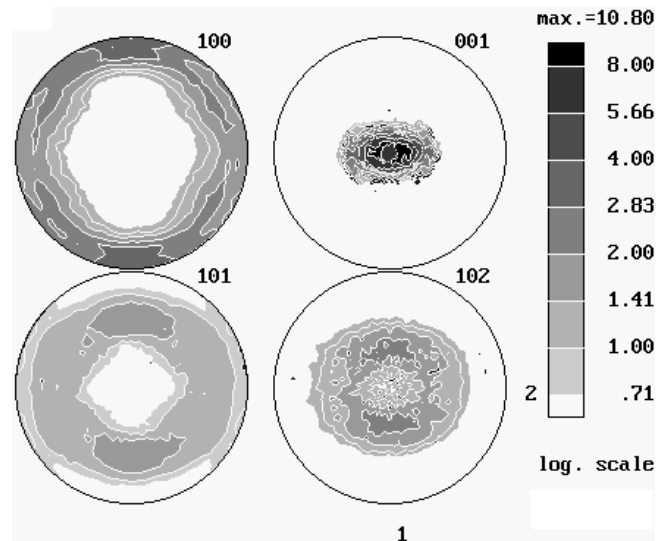


FIG. 4: Orientation maps of crystal planes in foils $125\ \mu\text{m}$ thick. Each circular figure is a stereographic projection, showing a greyscale map of the distribution of normals to one plane. The center of the circle is the normal to the sample; the circumference is the set of directions lying in the plane of the sample.

sample assembly was clamped by the edges, the holder having apertures for the drive and velocimetry beams. The holder was designed for use with a wide sample assembly, i.e. a large aperture for the sample, so that the clamp-type arrangement used to hold the sample would be well out of the region illuminated by the x-rays and thus unlikely to increase the x-ray background by fluorescence. Thus either a wide sample was used (~ 10 mm across), or the sample was attached to a retaining mount (e.g. a washer) of a material which would not cause problems with x-ray fluorescence. For the Be experiments, pieces were cut which were large enough to fill the full aperture in the holder.

C. Shock-driving beam

TRIDENT was operated in nanosecond mode, in which each pulse comprised up to 13 consecutive elements whose intensity was controlled separately. Using all elements, the drive pulse would be 2.5 ns long. For the time-resolved x-ray diffraction experiments reported here, the pulse length was shorter (fewer elements used) to optimize the efficiency of energy conversion to x-rays. The pulses generated were approximately square, with a slight ramp to induce a more constant pressure. The shock-driving beam was focused through a Fresnel zone plate to produce a uniform irradiance over a spot 5 mm in diameter [17]. The pulse energy and intensity history were recorded on each shot.

The power history delivered by each laser beam was

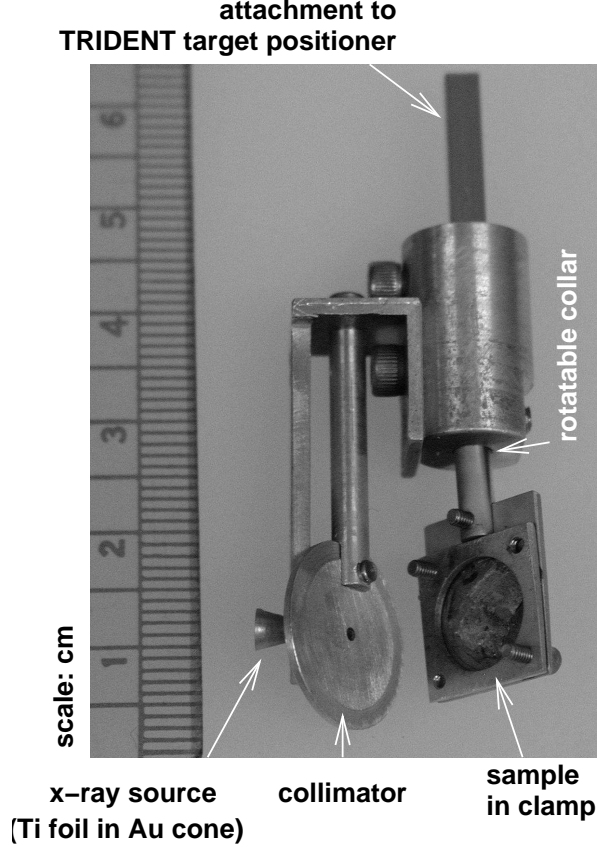


FIG. 5: Re-usable clamp-type target holder ('Ortiz holder').

measured in each experiment by directing the light reflected from uncoated glass plates in the beam path onto a fast photodiode and a calorimeter. The spatial distribution of laser in the target plane had been measured separately [17], and was used to convert the power history to the irradiance history. The calorimeter reading had been calibrated previously against a calorimeter placed at the center of the target chamber. The uncertainty in energy was of the order of 1 J.

D. Velocity history

For the supporting experiments without diffraction, the velocity history of the free surface of the sample was measured by time-resolved laser Doppler velocimetry, using a system of the 'velocity interferometry for surfaces of any reflectivity' (VISAR) type [18]. Line VISAR illumination was provided by a pulsed Nd:YAG laser, operating at 1319 nm wavelength with output frequency-doubled to 660 nm. The laser pulse was around 50 ns long. Line VISAR fringes were recorded using an optical streak camera. The fringe constant of the VISAR was computed from the thickness of the delay element (3" of SF6 glass). The dispersion of the glass was determined at

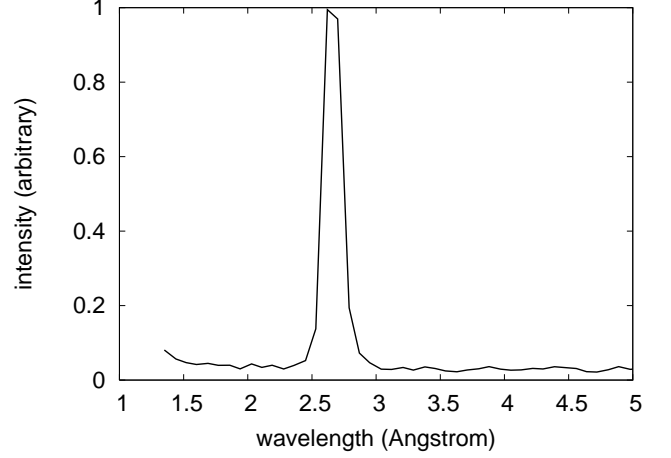


FIG. 6: X-ray spectrum from laser-heated Ti foil.

the wavelength of the probe laser by fitting a straight line to points sampling the variation of refractive index with wavelength. The fringe constant deduced was 806 m/s at 660 nm wavelength.

E. X-ray diffraction

The plasma x-ray source used one beam from TRIDENT, focused tightly ($\sim 150 \mu\text{m}$ diameter spot) on a metal foil $\sim 10 \mu\text{m}$ thick to generate a hot plasma. The plasma emitted He- α radiation from recombination of the ionized atoms. The x-ray spectrum was measured with a grating spectrometer, recording on Kodak Corp. DEF film and was thus a time-average over the duration of x-ray emission. The spectrum was essentially monochromatic for the range and precision of diffraction angles in these experiments (Fig. 6). The source material was chosen according to the anticipated x-ray diffraction angles: Ti (He- α at 2.61 \AA or 4.75 keV) for use with Be at compressions of up to a few tens of percent.

The plasma source emitted x-rays roughly isotropically into 4π steradians. The collimator was an Al disk, 1 mm thick and 15 mm in diameter. A hole 1 mm in diameter was drilled through the center to define the beam size. This rather large size was chosen so that a signal would be more likely to be observed in early trials. The collimator was twisted with respect to the x-ray axis in subsequent experiments to present a narrower (non-circular) aperture.

The orientation of the films and cameras was chosen so that diffraction from Be {0002} planes would be within the field of view. The energy in the laser beam heating the x-ray source was typically 150 to 200 J over 1.0 ns for a Ti source. The x-ray source foil was mounted inside a truncated gold cone, which prevented direct irradiation of the x-ray detectors by the source. The emission spectrum was recorded using a transmission grating and DEF film.

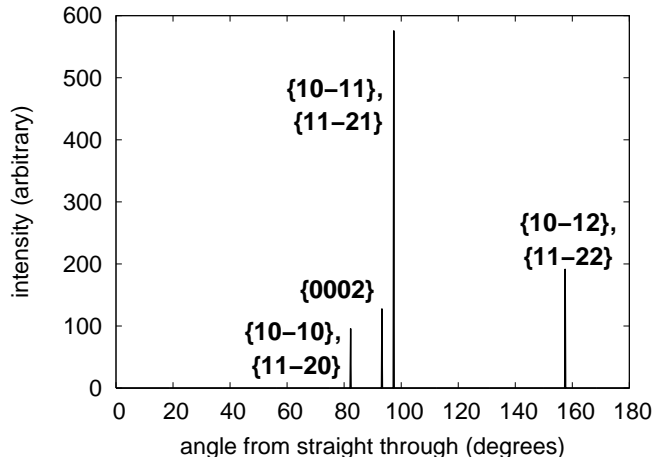


FIG. 7: Simulated powder pattern for polycrystalline Be.

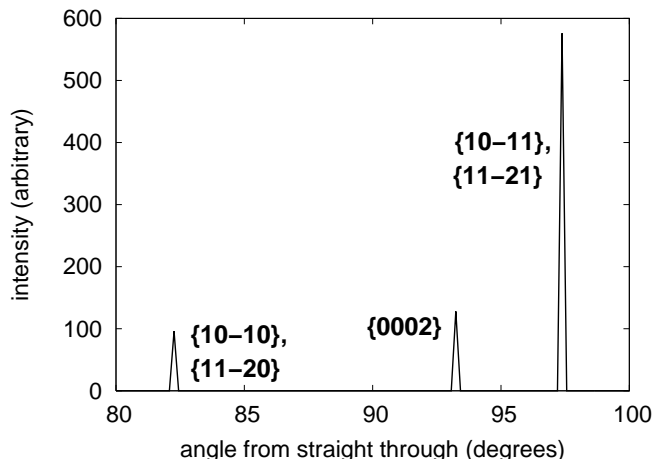


FIG. 8: Simulated powder pattern for polycrystalline Be (range of angles captured by detectors).

X-rays from the plasma were incident on the sample material, and diffracted from individual grains according to the Bragg condition. The attenuation length of ~ 5 keV x-rays in Be is several hundred microns, compared with sample thicknesses of a few tens of microns. Thus the diffraction signals were averages through the entire thickness of each sample, in general comprising material in different states of compression. If compressed material was present – e.g. behind the shock wave – during the backlighter pulse, the x-rays were diffracted at a different angle. If the grains in the sample were oriented isotropically, the powder diffraction pattern obtained with x-rays of the wavelength used in these experiments would comprise a cluster of three lines within 10° of 90° from the undiffracted beam (Figs 7 and 8).

Diffracted x-rays were recorded on DEF films (time-integrating) and Kentech x-ray streak cameras. The light

signal from the streak tube was amplified with an image intensifier before recording on TMAX optical film. In some cases, signals were observed on the x-ray streak cameras but not on the time-integrating films placed in front of the cameras, because the cameras were much more sensitive than the film. CsI photocathodes were used in the x-ray streak cameras. CsI is relatively sensitive but has a short life in experiments of this type: in some experiments, the CsI was damaged and produced spurious signals. The streak camera slits each subtended an angle of 12° at the target. The time-integrating films subtended an angle of 20° , constrained by the inside diameter of the cylindrical camera snout.

Filter foils were added to control the signal level, in front of the film pack, and between the film pack and the photocathode of the x-ray streak camera. $125\ \mu\text{m}$ of Be was used in all cases, with around $25\ \mu\text{m}$ of Ti, the exact thickness adjusted for best signal.

III. LOADING HISTORIES

The loading histories were calculated using a method described previously [12, 13, 17]. Radiation hydrodynamics simulations were used to predict the loading history applied to the sample, with the sample material treated as a fluid. The predicted loading history was then used as a time-dependent pressure boundary condition for continuum mechanics simulations in which elastic, plastic, and damage models were included for the sample material.

The experiments with surface velocimetry were used as the primary diagnostic to validate the simulations. These wave profile measurements yielded the timing and amplitude for any elastic precursor wave and the plastic shock, and the detailed pressure history.

A. Radiation hydrodynamics

As shown previously [12], ablative laser loading on nanosecond time scales with irradiances ~ 0.1 to $10\ \text{PW}/\text{m}^2$ can be simulated accurately by treating the ablation region ($\sim 1\ \mu\text{m}$ wide of the solid sample and the resulting plasma cloud) with three temperature hydrodynamics (ions, electrons, and radiation), thermal conduction and radiation diffusion, and laser absorption through the electrical conductivity. The remainder of the condensed phase was treated using non-radiative continuum mechanics, i.e. with an equation of state (EOS) and a constitutive model. Some specific processes excluded in this plasma model, i.e. negligible in the regime considered, include resonant absorption, transport of the resulting hot electrons, and generation, transport, and deposition of Bremsstrahlung x-rays.

Simulations were performed using the HYADES radiation hydrocode, version 01.05.11 [19]. This hydrocode used a 1D Lagrangian discretization of the material, and

leapfrog time integration, and did not include material strength in the solid sample. Shock waves were stabilized using artificial viscosity. The EOS and opacity were represented using tabular models from the SESAME database [20]. Conductivities for laser deposition and heat conduction were calculated using the Thomas-Fermi ionization model [19, 21]; this was found previously to be reasonably accurate for direct drive shock simulations on samples of a wide range of atomic numbers [12]. The flux limiter was set to 0.03 of the free stream value - a common choice for simulations of this type [22].

The initial spatial mesh was set up to be expanding, to allow adequate resolution of the material to be ablated. Moving away from the sample surface, adjacent cells were expanded by 5%. The cell closest to the surface was 5 nm wide. Previous sensitivity studies had demonstrated that this resolution was adequate for direct drive simulations in this regime of irradiance and time scale [12]. Where possible, simulations were performed using the irradiance history measured on each shot to infer the precise loading history applied to each sample. The exceptions were experiments in which the photodiode measuring drive history was saturated; in these cases, the shape was assumed to be the same as for shots fired shortly before or after, and the amplitude was scaled to give the correct total energy. The raw photodiode record was converted to irradiance by scaling so that the integral under the curve matched the measured pulse energy, and dividing by the area of the focal spot. The raw record contained high frequency fluctuations, giving negative apparent values of the irradiance when the signal was low. For the simulations, the inferred irradiance history was reduced to a piecewise linear variation reproducing the principal features to a few percent in instantaneous irradiance.

B. Continuum mechanics

Continuum mechanics simulations were used to predict the propagation and evolution of the loading history through the thickness of the sample, taking account of the constitutive properties (elasticity and strength) of the material. Simulations were performed using the LAGC1D hydrocode, version 5.2 [23]. This hydrocode used a 1D Lagrangian discretization of the material, and predictor-corrector time integration. Shock waves were stabilized using artificial viscosity.

IV. RESULTS

These experiments were performed at the TRIDENT laser facility during July-August 2000, July-August 2001, and August 2002 ('Flying Pig 2' shot series). For the pulses nominally 1.0 and 1.8 ns long, the laser pulse comprised 6 and 9 elements respectively. No-shock test shots were performed to check the signal level in static diffraction with the nanosecond laser-heated x-

ray source, and to optimize camera gain and filtering. Dynamic shots were performed with shock pressures between 10 and 50 GPa. Some shots were performed with similar shock conditions to check reproducibility. On a few shots, the irradiance history of the shock-driving beam exhibited significant, undesired variations. On the remainder, the irradiance was close to the desired history, and the shock-driving pressure was constant to within around 10%.

A. Static trials

With no shock drive, a clear diffraction signal was observed from the $\{0002\}$ planes, as a line on the time-resolved streak camera record (Fig. 9, and as an arc on the time-integrated film (Fig. 10). The arc was mottled, presumably corresponding to diffraction from specific favorably-oriented grains in the sample. The arc was the visible part of the conic section between the cone of diffracted x-rays and the film plane; the rest of the curve was obscured by the streak camera snout, which was in front of the cassette for the time-integrating film. Apart from the desired diffraction line, there was no significant x-ray exposure above the background fog level of the film, indicating that scatter or fluorescence from Al and steel components in the target holder was not a problem. The breadth of the arc, and the width of the time-resolved line, varied with the width of the beam passed by the collimator. The incident beam was adjusted so that the doublet in the x-ray source spectrum was visible in the x-ray streak record.

The target chamber geometry constrained the location of the 'Laue' streak camera and the static film mount attached to its snout so that unshocked lines were barely visible at the extreme ends of the static field of view.

B. Shock trials

With a shock drive, one or more displaced arcs appeared on the time-integrated film (Fig. 11), and one or more additional lines appeared on the streak camera record (Fig. 12). Clearest results were obtained for shock pressures around 10-20 GPa (Fig. 13). At higher pressures, the diffraction lines passed out of the field of view of the detectors. In general, the x-ray streak record showed a sharp unshocked line, growing weaker as the shock compressed more material; diffraction from shocked material, less sharp than the unshocked line presumably because of the slightly varying shock pressure; and a sharp line from released material with a lattice parameter slightly greater than that of the unshocked material. The displacement of the $\{0002\}$ Bragg reflection was consistent between the time-resolved and time-integrated measurements, but could be measured more accurately from the time-resolved record.

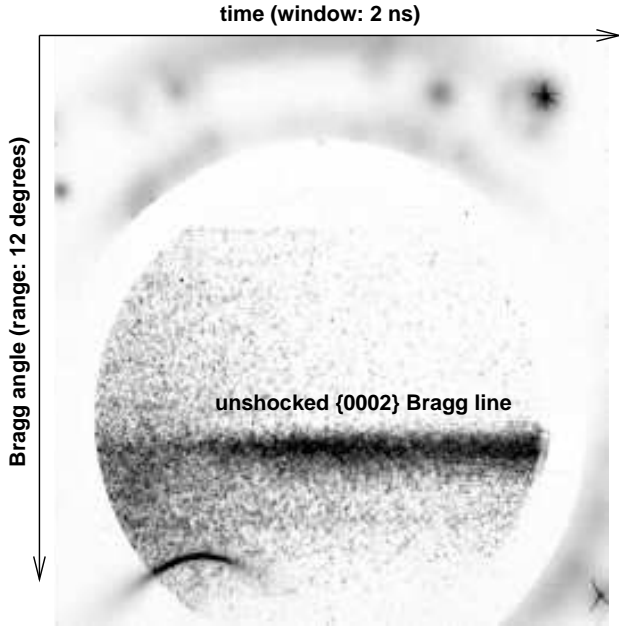


FIG. 9: Example x-ray streak camera record from a static (unshocked) trial: TRIDENT shot 13664. The spots and star-shaped markings at the outside were caused by arcing from the pulsed high voltage in the streak tube. The circular image intensifier is clearly evident.

One complication in interpreting the shocked signal was that material compressed uniaxially in the elastic precursor wave had a similar lattice parameter to material compressed more isotropically in the plastic wave. The amplitude of the elastic wave was observed clearly in the line VISAR measurements of free surface velocity history (Fig. 14).

V. INTERPRETATION OF DIFFRACTION LINES

The interpretation of a single diffraction line in the absence of other data depends on the assumed orientation of the plane with respect to the shock, and on the assumed symmetry of deformation of the lattice. The extreme cases of lattice deformation are pure uniaxial or pure isotropic, and this assumption leads to significant differences in the compression or stress inferred from a given change in diffraction angle (Fig. 15).

Pure uniaxial lattice deformation occurs in elastic waves only; pure isotropic deformation occurs when the flow stress is negligible. When the drive pressure is not high enough to overdrive the elastic precursor, the diffraction signal would in principle consist of uniaxial compression to the elastic strain corresponding to the flow stress, and partially-isotropic compression to the highest pressure. Plastic flow acts to return the elastic strain to the flow stress, so the high pressure state gen-

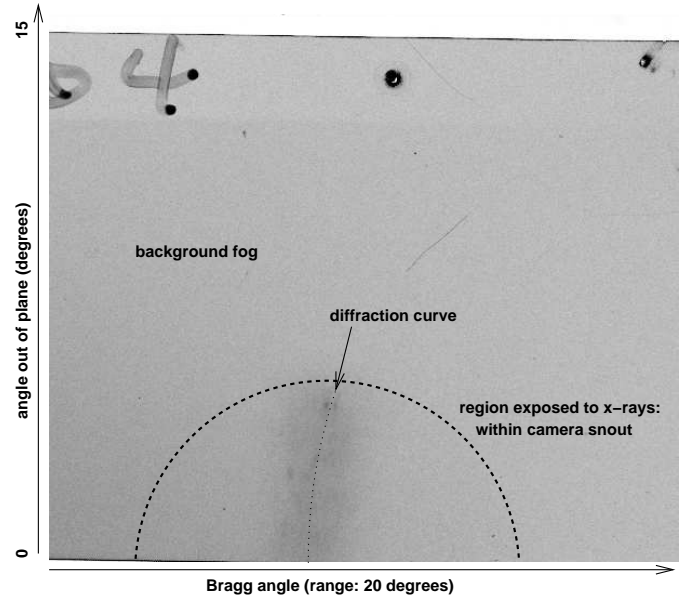


FIG. 10: Example x-ray film record from a static (unshocked) trial: TRIDENT shot 15004.

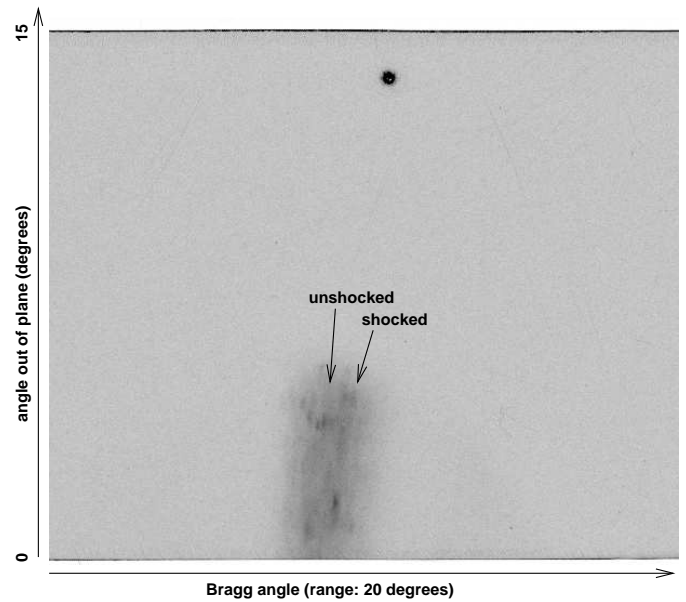


FIG. 11: Example x-ray film record from a shocked sample: TRIDENT shot 15002.

erally includes a uniaxial component of this magnitude rather than pure isotropic compression. (The isotropic stress state is generally not an isotropic strain state for a single crystal, as the elastic constants generally vary with orientation.) When the drive pressure is high enough to overdrive the elastic wave, the high-pressure state is of course all that would be observed. If the elastic wave reaches an impedance mismatch at the opposite surface of the sample (e.g. and usually a free surface), it will

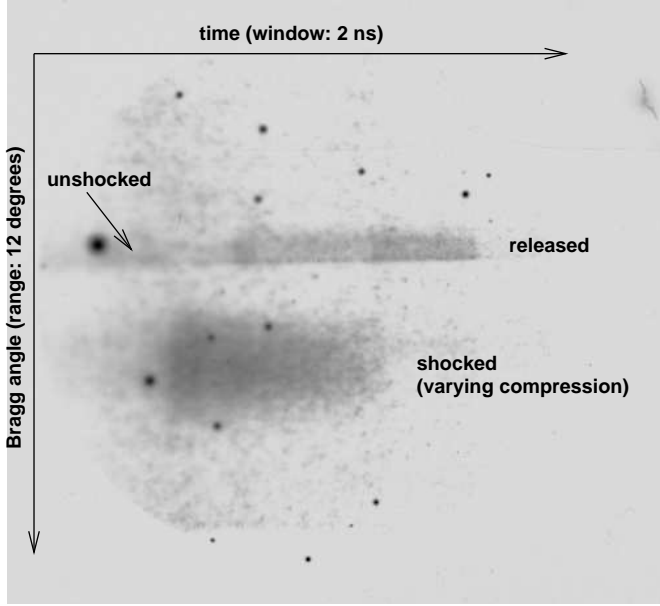


FIG. 12: Example x-ray streak camera record from a shocked sample: TRIDENT shot 15002.

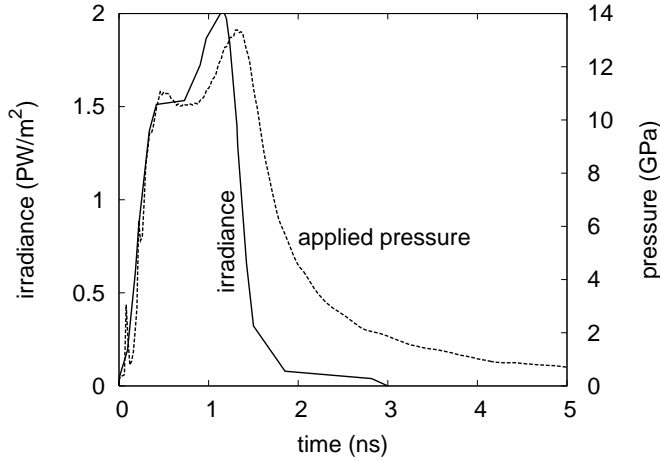


FIG. 13: Irradiance and drive pressure history from example dynamic loading experiment (TRIDENT shot 15002).

reverberate between the surface and the plastic shock, creating regions of intermediate strain.

When interpreting time-resolved and time-integrated records, the detailed signal depends on the timing of the x-ray pulse with respect to the propagation of the different waves and the range of penetration of the x-rays in the sample. For Be, x-rays of the energy used here can penetrate hundreds of microns, so the diffraction signal was integrated over all positions through the thickness of the sample.

The time-resolved Bragg records typically showed a strong doublet near the center, again from (0002) planes.

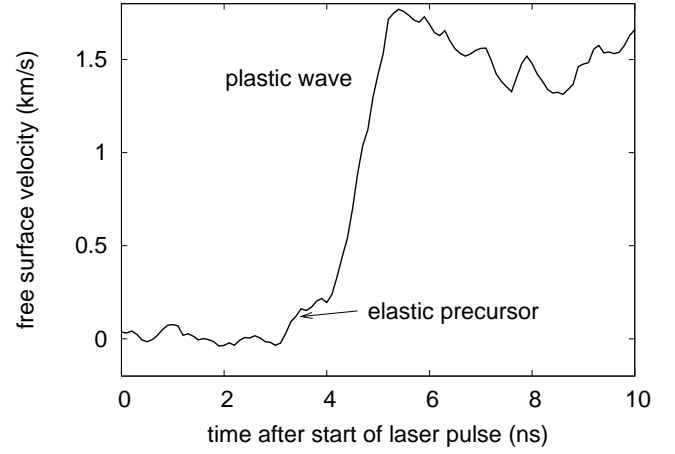


FIG. 14: Example free surface velocity history from a shocked sample: TRIDENT shot 12182.

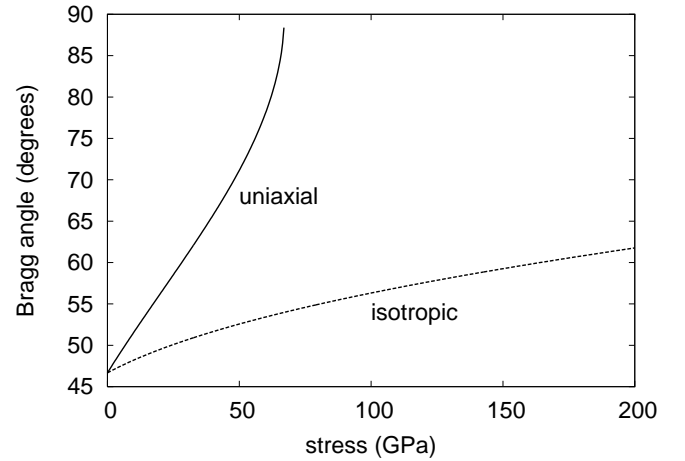


FIG. 15: Dependence of (0002) Bragg angle in Be on shock pressure, for limiting assumptions about the deformation symmetry of the lattice.

In experiments with shock loading, the time-resolved Bragg records also showed a broad signal corresponding to lattice compression. The degree of compression can be converted to a uniaxial stress or an isotropic pressure by assuming a degree of uniaxiality. Assuming uniaxial strain around the [0001] direction, the range of angles in for example shot 15002 implied a flow stress in the range 3 to 8 GPa, which is consistent with values deduced from velocimetry. Assuming isotropic compression, the range of angles implied a shock pressure in the range 7 to 20 GPa, bracketing the expected shock pressure but with a much larger range than expected for any individual experiment. Unfortunately, the Bragg angles expected for uniaxial and isotropic compression in this range were fairly similar: the observed record is certainly a superposition of both types of deformation. This ambi-

guity should be absent in the higher-compression experiments needed to investigate shock-induced melting, as the Bragg angles would be significantly different and the elastic wave may be overdriven in many cases; a wider field of view would be needed to detect Bragg angles over the necessary range of compressions. The ambiguity would also be less in experiments on softer materials. In shot 15012, the shocked signal moved with time, possibly indicating lattice relaxation i.e. the transition from uniaxial to isotropic compression. The drive pressure was predicted to be relatively constant (compared with the change in lattice parameter); it seems possible that the signal has captured the decay of a very strong elastic precursor (~ 10 GPa) at early times.

The time-integrated Laue records typically showed two faint signals close to the edges of the field of view, i.e. around 15° apart. The position and spacing are consistent with the $\{10\bar{1}0\}$ and $\{11\bar{2}0\}$ lines at one edge and the $\{10\bar{1}1\}$ and $\{11\bar{2}1\}$ lines at the other. Presumably the $\{0002\}$ lines did not appear – and the lines above did not appear on the Bragg record – because of the texture of the rolled foils. The position and low signal levels made it difficult to extract any useful distribution of angles.

VI. DISCUSSION

Experiments were performed in which Be foils were loaded by laser ablation, and the distortion of the grains was monitored with *in situ* x-ray diffraction. X-ray powder patterns were clearly visible on the time-integrated (film) record positioned to capture reflections from $\{0002\}$ planes, and there was evidence of lines at

the edges of the opposite time-integrating record, consistent with diffraction from $\{10\bar{1}0\}$, $\{11\bar{2}0\}$, $\{10\bar{1}1\}$, and $\{11\bar{2}1\}$ planes. In some experiments, the x-ray streak cameras also recorded diffraction lines, but some apparent lines may have been caused by camera faults. The records clearly included signals from shocked and unshocked Be. The deviations in Bragg angle were consistent with strains anticipated from the ablative loading applied, and the range of flow stress deduced from surface velocimetry. In these initial experiments, the accuracy and separation of the changing diffraction lines was not sufficient to be used in isolation – velocimetry is essential, and a wider angular coverage for x-ray detection is highly desirable. The measurements did unambiguously demonstrate diffraction from shocked, polycrystalline material.

Acknowledgments

We would like to thank the TRIDENT staff, particularly Randy Johnson, Tom Hurry, Tom Ortiz, Fred Archuleta, Nathan Okamoto, and Ray Gonzales, for their hard work on the experiments. Bernie Carpenter (P-24) and Kathy Gallegos (Bechtel) scanned the films. Jon Larsen (Cascade Applied Sciences, Inc.) gave advice on the use of the radiation hydrocode HYADES.

Funding was provided by Allan Hauer and Steve Batha of the LANL Program Office for the National Nuclear Security Administration's Campaign 10, Inertial Confinement Fusion. The work was performed under the auspices of the U.S. Department of Energy under contract W-7405-ENG-36.

-
- [1] M.I. Emerets, 'High Pressure Experimental Methods' (Oxford Science, London, 1996).
 - [2] Q. Johnson, A. Mitchell, R.N. Keeler, and L. Evans, Phys. Rev. Lett. **25**, 1099 (1970).
 - [3] P.A. Rigg and Y.M. Gupta, Phys. Rev. B **63**, 9, 094112 (2001).
 - [4] A. Loveridge, A. Allen, D. Kalantar, B. Remington, R.W. Lee, S. Weber, A. Hauer, G. Kyrala, D. Paisley, B. Holian, P. Lomdahl, T. Boehly, M.A. Meyers, D.C. Swift, J.S. Wark, Phys. Rev. Lett. **86**, 2349 (2001).
 - [5] C. Rose-Petruck, R. Jimenez, T. Guo, A. Cavalleri, C.W. Siders, F. Raksi, J.A. Squier, B.C. Walker, K.R. Wilson, C.P.J. Barty, **398**, 310 (1999).
 - [6] H. Kishimura, A. Yazaki, H. Kawano, Y. Hironaka, K.G. Yakamura, and K. Kondo, J. Chem. Phys. **117**, 22, 10239 (2002).
 - [7] D.C. Swift, G.J. Ackland, A. Hauer, and G.A. Kyrala, Phys. Rev. B **64**, 214107 (2001).
 - [8] D.C. Swift, D.L. Paisley, G.A. Kyrala and A. Hauer, shocks in Proc. American Physical Society Topical Conference on Shock Compression of Condensed Matter, held Atlanta, GA, 25-29 Jun 2001; AIP CP620 (2002).
 - [9] D.C. Wilson et al, Phys. Plasmas **5**, 5, pp 1953-9 (1998).
 - [10] P.A. Bradley and D.C. Wilson, Phys. Plasmas **6**, 11, pp 4293-303 (1999).
 - [11] J.D. Lindl, "Inertial confinement fusion" (Springer-Verlag, New York, 1998).
 - [12] D.C. Swift, T.E. Tierney IV, R.A. Kopp, and J.T. Gammel, Phys. Rev. E **69**, 036406 (2004).
 - [13] D.C. Swift, J.T. Gammel, and S.M. Clegg, Phys. Rev. E **69**, 056401 (2004).
 - [14] D.C. Swift, *Laser-induced shock experiments on Be foils*, Los Alamos National Laboratory report LA-UR-01-6430 (2001).
 - [15] D.C. Swift, *Simulations of ablatively-driven shock wave experiments on Be (TRIDENT experiments: July-August 2000)*, Los Alamos National Laboratory report LA-UR-04-7411 (2004).
 - [16] D. McKie and C. McKie, "Crystalline Solids" (Nelson, Walton-on-Thames, 1974).
 - [17] D.C. Swift and R.P. Johnson, Phys. Rev. E **71**, 066401 (2005).
 - [18] L.M. Barker and R.E. Hollenbach, J. Appl. Phys. **43**, 4669 (1972).
 - [19] Documentation for HYADES computer program, version 01.05.11 (Cascade Applied Sciences Inc, Golden, Col-

- orado, 1998).
- [20] S.P. Lyon and J.D. Johnson (Los Alamos National Laboratory), *SESAME: the Los Alamos National Laboratory equation of state database*, Los Alamos National Laboratory report LA-UR-92-3407 (1992).
- [21] Ya.B. Zel'dovich and Yu.P. Raizer, "Physics of shock waves and high temperature hydrodynamic phenomena" (Academic Press, New York, 1966).
- [22] R. Dendy, "Plasma Physics" (Cambridge University Press, Cambridge, 1993).
- [23] Documentation for LAGC1D computer program, version 5.2 (incorporating ARIADNE material properties library, version 7.0, and C++ mathematical class library, version 2.0), (Wessex Scientific and Technical Services Ltd, Perth, Scotland, 2003; <http://www.wxres.com>).